Developmental Cell, Vol. 5, 583–594, October, 2003, Copyright ©2003 by Cell Press

ER-to-Golgi Carriers Arise through Direct En Bloc Protrusion and Multistage Maturation of Specialized ER Exit Domains

Alexander A. Mironov,[1,6] Alexander A. Mironov, Jr.,[1,6] Galina V. Beznoussenko,[1] Alvar Trucco,[1] Pietro Lupetti,[2] Jeffrey D. Smith,[3] Willie J.C. Geerts,[4] Abraham J. Koster,[4] Koert N.J. Burger,[4] Maryann E. Martone,[5] Thomas J. Deerinck,[5] Mark H. Ellisman,[5,7] and Alberto Luini[1,7,*]

[1]Department of Cell Biology and Oncology
Istituto di Ricerche Farmacologiche "Mario Negri"
Consorzio Mario Negri Sud
66030 Santa Maria Imbaro (Chieti)
Italy

[2]Dipartimento di Biologia Evolutiva
Università di Siena
53100 Siena
Italy

[3]NASA Ames Research Center
Moffett Field, California 94035

[4]Department of Molecular Cell Biology
Institute of Biomembranes
Utrecht University
3584 CX Utrecht
The Netherlands

[5]National Center for Microscopy and Imaging Research
University of California, San Diego
La Jolla, California 92037

Summary

Protein transport between the ER and the Golgi in mammalian cells occurs via large pleiomorphic carriers, and most current models suggest that these are formed by the fusion of small ER-derived COPII vesicles. We have examined the dynamics and structural features of these carriers during and after their formation from the ER by correlative video/light electron microscopy and tomography. We found that saccular carriers containing either the large supramolecular cargo procollagen or the small diffusible cargo protein VSVG arise through cargo concentration and direct en bloc protrusion of specialized ER domains in the vicinity of COPII-coated exit sites. This formation process is COPII dependent but does not involve budding and fusion of COPII-dependent vesicles. Fully protruded saccules then move centripetally, evolving into one of two types of carriers (with distinct kinetic and structural features). These findings provide an alternative framework for analysis of ER-to-Golgi traffic.

Introduction

Traffic between the ER and the Golgi in animal cells is mediated by large pleiomorphic tubular-vesicular structures (Presley et al., 1997; Scales et al., 1997). It remains unclear how these structures arise from the ER, how they discharge cargo into the Golgi complex, and whether the ER-to-Golgi carriers (later referred to as "carriers") represent transient transport intermediates that are constantly forming from the ER and being consumed at the *cis*-Golgi pole, or a more stable compartment shuttling back and forth between the ER and the Golgi (Klumperman, 2000).

A scheme that has so far enjoyed a wide consensus posits that these carriers form through budding from the ER of many small (60 nm) coat protein II (COPII)-dependent vesicles, followed by their homotypic fusion into a larger container (Ladinsky et al., 1999; Klumperman, 2000; Horstmann et al., 2002). However, this model does not easily explain the transport of large macromolecular cargo, such as long (>300 nm) rigid trimers of procollagen I (PC) in fibroblasts (Bonfanti et al., 1998) and lipid droplets (40–200 nm in diameter) in hepatocytes and enterocytes (Claude, 1970; Sabesin and Frase, 1977; see also Krijnse-Locker et al., 1995 and Rambourg and Clermont, 1997). Such cargoes are formed in the lumen of the ER and are too large to fit into 60 nm COPII vesicles. This discrepancy can, in principle, be overcome by the proposal that the COPII machinery might be sufficiently flexible as to accommodate large particles, and COPII vesicles of up to 85 nm in diameter have indeed been observed (Antonny and Schekman, 2001). Nevertheless, the fact that cargoes such as PC can exit the ER as large aggregates (300–400 nm in length) suggests, prima facie, that a different mechanism might apply, perhaps involving the en bloc extrusion of large, ER cargo-containing domains.

Here, we report that the carriers containing PC and those carrying the temperature-sensitive G protein variant of the vesicular stomatitis virus (VSVG; as a small diffusible molecule that can potentially enter vesicles) both form by protruding en bloc from specific areas of the ER membrane without the participation of small vesicles. Both then evolve into translocating carriers through multiple maturation stages.

Results

The formation of ER-to-Golgi carriers was analyzed using two synchronizable secretory proteins as traffic markers: the macromolecular cargo PC, which is too large to fit into COPII vesicles (Bonfanti et al., 1998), and the small diffusible viral protein VSVG, which can potentially enter such vesicles. Human fibroblasts (HFs) and chick embryonic fibroblasts (CEFs) are professional PC secretors and are suitable for the synchronization of PC and VSVG traffic in the same cell (Mironov et al., 2001).

Four Main Ultrastructural Types of ER-to-Golgi Carriers

The exit of PC from the ER of HFs and CEFs was synchronized by blocking PC hydroxylation, as previously described (Bonfanti et al., 1998; Mironov et al., 2001;

*Correspondence: luini@negrisud.it
[6]These authors contributed equally to this work.
[7]Principal investigators.

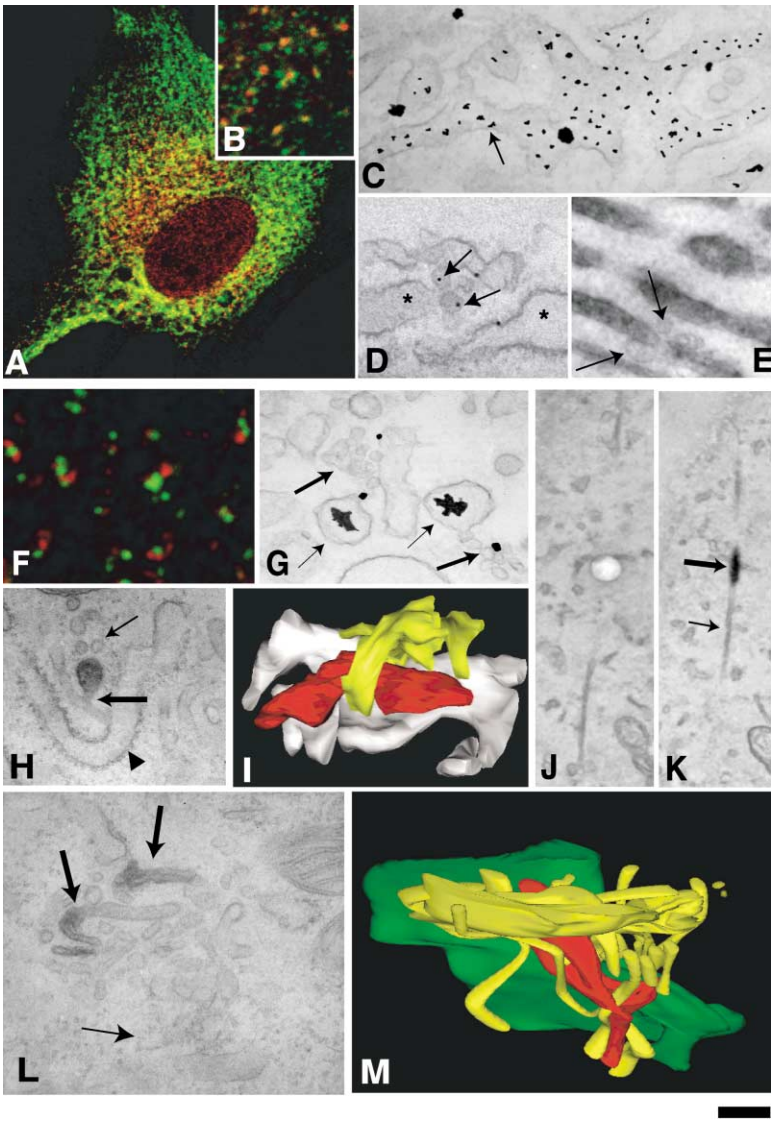

Figure 1. Structure of PC-Containing Carriers

HFs (A, D, and E) and CEFs (B and C) were subjected to hydroxylation blocks (HFs, 1% calf serum in the absence of ascorbic acid at 40°C for 3 hr; CEFs, 0.3 mM dipyridyl [see Bonfanti et al., 1998] for 1 hr). Cells were fixed at 0 (A and C–E), 4 (B), or 10 min (F–M) after hydroxylation block release (HFs, 32°C + 50 μM ascorbic acid; CEFs, after dipyridyl washout) and prepared for IF or IEM. Three-dimensional reconstruction and surface rendering of PC containers was performed on delineated serial sections.

(A) ER-like pattern of the PC labeling before the release of the block (0 min). No colocalization of PC (green) is seen with Sec31 (red). PC colocalizes with calreticulin (not shown).

(B) Four minutes after the release of the transport block, PC is in spots (green) that do not colocalize with Sec31 (red).

(C) Diffuse distribution of PC (enhanced gold particles, arrow) through ER cisternae.

(D) Distribution of Sec31 (enhanced gold particles, arrows) at an ERES and at ER cisternae (asterisks).

(E) PC (DAB precipitate) is abundant in distended ER cisternae, whereas an ERES (arrows) is devoid of PC.

(F) Ten minutes after the block release, folded PC (green) appears as spots offset from Sec31-positive spots (red).

(G) PC (thin arrows) at the EM level is visible as gold aggregates in distended ER domains near ERESs (thick arrows). The PC staining does not have the diffuse ER appearance seen in (C).

(H) The type II carrier. The PC container is connected (thick arrow) with the ER (arrowhead). Profiles of the ERES (thin arrow) do not contain PC.

(I) Three-dimensional view of the type II carrier shown in (C). The PC-positive container is in red, and the ER is in white. The PC-negative container is in yellow.

(J and K) Type III carrier. Serial sections of the tangential tubule (thin arrow) containing a varicosity with PC (DAB precipitate; thick arrow).

(L) Type IV carrier. Two saccules are filled with PC (thick arrows), whereas profiles of an ERES (thin arrow) do not contain PC.

(M) Three-dimensional view of the type IV carrier shown in (H). The ERES is in yellow, the ER in green, and the PC-positive container is in red.

The scale bars represent 5 μm (A), 2 μm (B and F), 100 nm (C–E and L), 200 nm (G and H), and 350 nm (J and K).

see legend to Figure 1). This block was then released, and the cells were examined after 0, 4, and 10 min. At time 0, by immunofluorescence (IF), unfolded PC exhibited the predictable diffuse, reticular distribution (Figure 1A) and could not be detected by the LF68 antibody against folded PC (not shown). In corresponding EM images, PC was homogeneously distributed throughout the distended cisternae of the ER (Figure 1C). Four minutes after the release of the folding block, PC began to concentrate in dots of varying brightness (typically 3-fold higher than that of the surrounding ER) that were scattered throughout the cytoplasm. They were detectable by the antibody against folded PC (not shown), indicating that PC folding was taking place. These dots were very close to, but usually not overlapping with, the COPII-labeled ER exit sites (ERESs; Figure 1B). The ERESs (using antibodies against either Sec23 or Sec31, subunits of the COPII coat) appeared as bright roundish spots of an apparent diameter of 0.5–1.0 μm that were scattered throughout the cell and numbered between 100 and 200 (Figures 1A and 1B). In thin EM sections, the ERESs were seen as small clusters of three to ten round-to-ovoid profiles that labeled for COPII (Figure 1D), and PC appeared concentrated in distended domains of the ER of 600–800 nm in diameter that were located close to (within 0.5 μm), and continuous with, ERESs attached to the ER cisternae (Figure 1E).

Ten minutes after the release of the block, a subset of PC carriers had left the ERESs and reached the Golgi; however, other PC carriers were still scattered in the

cell periphery (not shown). In contrast, the ERESs had not changed in number and distribution. At the EM level, the PC-positive structures (carriers) could be subdivided into four categories (see below for a schematic representation). Type I: distended domains of the ER located close (from a few nm to 0.5 μm) to an ERES (Figures 1F and 1G). These structures were very similar to those seen at 4 min (above) and are therefore likely to be containers seen just in the process of appearing from the ER. Type II: flattened and elongated (>300 nm) saccules protruding from, but still in continuity through tubules with, the ER (Figures 1H and 1I). The saccules had average dimensions of 350 by 150 nm (i.e., large enough to contain 300 nm long PC trimers) and were still in the vicinity of (within 0.5 μm), and often continuous with, an ERES. The main difference between containers of types I and II was that the former were embedded in the ER cisterna, whereas the latter had protruded out and were clearly segregated from the ER cisterna, although always associated/connected with it by tubules. Thus, type II structures probably represent carriers after protrusion from the ER (see below). Remarkably, the type I and II PC saccular carriers were devoid of COPII labeling, which, in contrast, was intense on the adjacent ERES (Figure 1F; see also Figure 1B and Discussion). Very few bona fide buds were present in these regions. Type III: distensions (>300 nm in length) embedded in thin (50–70 nm) tubules devoid of ribosomes, which were usually radially oriented. These structures were uncommon, and were visible only in tangential thick (or serial) EM sections (Figures 1J and 1K). As shown later, they appear to be carriers caught during translocation toward the Golgi. Type IV: larger and more complicated membranes comprising several (two to four) saccules partially stacked. These saccules are often associated with aggregates of oval and elongated profiles and with the ER (Figures 1L and 1M). The same four types of PC containers were visible at steady state both in HFs and CEFs (unpublished observations).

Next, VSVG-containing carriers were examined in HFs or COS7, RBL, or NRK cells, which were infected with 045VSV and left to accumulate VSVG in the ER at the restrictive temperature (40°C) for 3 hr. Cells were then shifted to the permissive temperature (32°C) to allow VSVG to exit the ER, and fixed at 0, 4, and 10 min after release of the block. Although VSVG is a small diffusible molecule (Nehls et al., 2000) that can potentially enter small transport vesicles, the overall structures of its carriers were very similar to those just described for PC. The differences were few, as follows. First, at time 0, in VSVG-expressing cells, there was a high background of reticular COPII fluorescence in IF images (Figures 2A–2C), and in the corresponding EM images, COPII was present not only on ERESs, but also over ER domains (Figure 2D). This diffuse COPII labeling was absent in PC-secreting cells (see above) and might be due to binding of Sec23 to the cytosolic tail of VSVG (Aridor et al., 1998), which at this time is distributed throughout the ER. Indeed, 4 min after release of the folding block, when VSVG had begun to concentrate in spots that partially overlapped with the COPII-labeled ERESs (Figures 2H, 2I, and 2K; see Figure 2M for quantification), the COPII background disappeared as the Sec23/31 signal concentrated exclusively at the ERESs, in parallel with VSVG (Figure 2J). A second difference was that the forming VSVG carriers were positive for COPII (Figures 2E, 2F, and 2L; for immuno-EM, see below; at variance with PC-containing carriers; see above), possibly again as a consequence of binding between VSVG and COPII. Third, while PC was never detected in ERESs, VSVG was usually found to fill a portion of the adjacent ERES (Figures 3A and 3B).

In these VSVG carriers, we also examined the localization of COPI. COPI was found in types II and IV carriers (see below). In detail, in type II carriers, COPI was absent from the main saccular body and was concentrated at the isthmus of the protruding containers (Figure 2G). This observation is consistent with our own and with previously published IF details (Stephens and Pepperkok, 2002).

A notable similarity between VSVG- and PC-containing carriers was that only a very few vesicles and buds (which were devoid of cargo) were seen in the vicinity of both containers, and that type I and type II carriers appeared to be connected with the ER (33 VSVG carriers and 27 PC carriers were analyzed; see Figures 3B–3H).

To verify the observation that many carriers were connected to the ER, stereo-tilting analysis or electron tomography were used (Figures 3I and 3J), the latter of which provides a 3D resolution on the order of 5–7 nm. This eliminates most of the ambiguities of 3D reconstructions from serial sections. Nine VSVG containers were immunoperoxidase labeled and subjected to electron tomography (e.g., Figures 3I and 3J), and 33 VSVG containers and 13 PC containers (type II) were subjected to double or single tilting and stereo pair analysis. All the type II carriers showed connectivity, and all the type IV carriers showed association, with the ER (Figures 3D and 3G). In these images, we also noted that the structures appearing as buds in single sections were revealed in the 3D reconstructions of the ERESs to result from oblique sections of tubules. Bona fide buds were few. Round (potentially vesicular) profiles (see Experimental Procedures for definition) were also analyzed by tomography. Out of 174 round profiles analyzed in random virtual sections from four tomograms only 27 were found to derive from vesicles, rather than from other structures. These data indicate that in routine 60 nm sections most round profiles correspond to structures different from vesicles, and confirm that very few true vesicles are associated with ER exit domains. Additionally, to eliminate chemical fixation artifacts, samples were examined after rapid freezing-cryosubstitution (McIntosh, 2001). Because the low contrast of sections hampered recognition of carriers in thick sections, ultrathin (25–30 nm) serial sections were used instead of electron tomography (Figure 3K). In these samples, which cannot be immunolabeled, it was possible to unambiguously recognize only type II carriers. These carriers were not substantially different from type II carriers seen in fixed and immunostained cells (irregular saccules in continuity with the ER), except that they contained some pores and exhibited a more "blebby" surface (compare Figure 3L with Figure 3F).

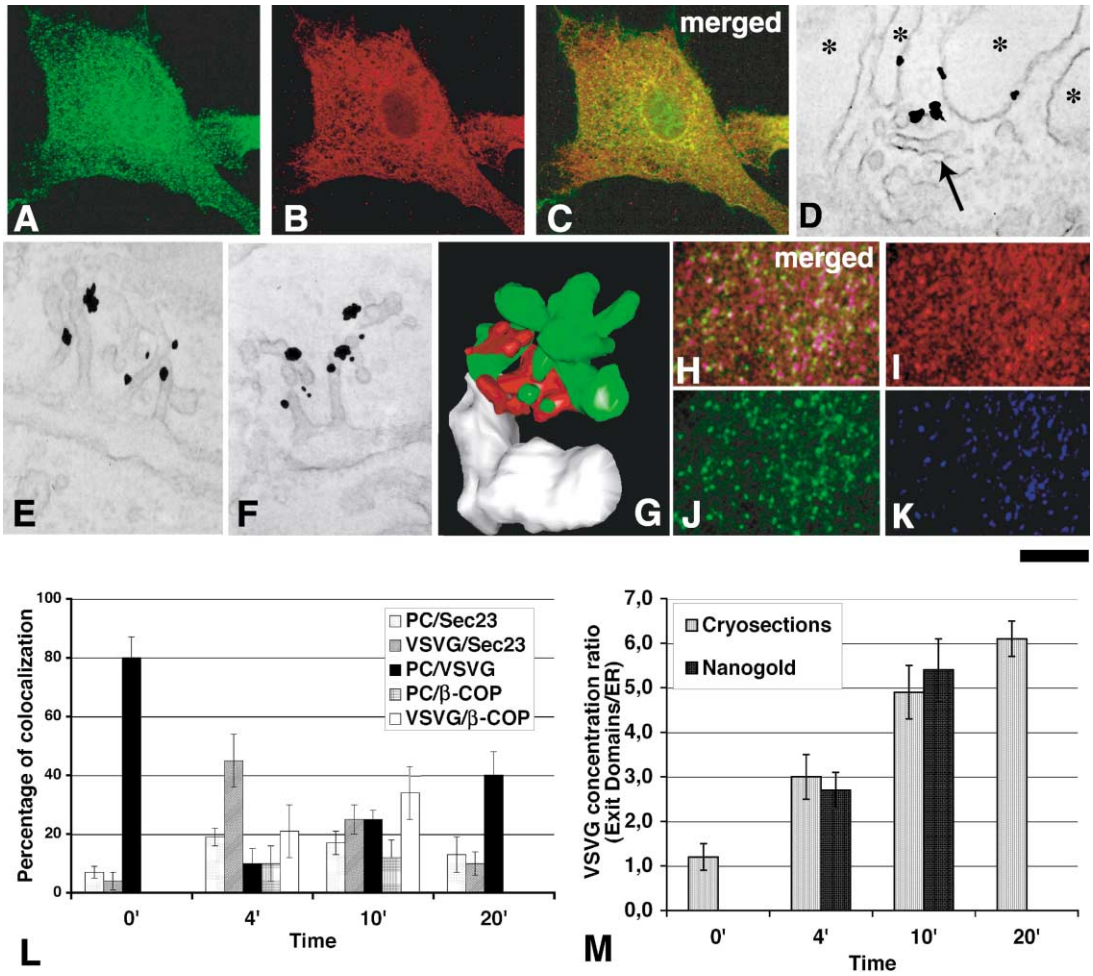

Figure 2. Initial Stages of VSVG Exit from the ER

HFs (A–D) and COS7 (E–K) cells were infected with 045VSV, placed at 40°C for 3 hr to accumulate VSVG in the ER (HFs were grown in the presence of 10% FCS to inhibit the synthesis of PC), shifted back to 32°C, fixed 0 (A–D) or 4 (E–K) min after the release of the temperature block, and prepared for IF or IEM.

(A–C) Reticular pattern of VSVG ([B and C], red) and no colocalization with Sec31 ([A and C], green). Sec 31 reveals a significant background.

(D) Sec31 labeling of ER cisternae (asterisks) adjacent to an ERES (arrow).

(E and F) Emanation of tubules positive for VSVG (E) and Sec31 (F) from the ER 4 min after the release of the temperature block.

(G) Three-dimensional representation of COPI localization by immunoperoxidase, in the presence of 12% gelatin to prevent diffusion of the DAB precipitate. Analogous results were obtained by nanogold labeling.

(H–K) Concentration of total VSVG ([I]; red, detection with anti-cytosolic domain antibodies), folded VSVG ([K]; blue, detection with I-14 antibodies; Lefrancois and Lyles, 1983), and ERESs ([J]; green, labeled with anti-Sec23). Both unfolded and folded VSVG are concentrated at ERESs. Diffuse VSVG staining is barely detectable only for the unfolded form.

(L) Colocalization of PC, VSVG, COPII (Sec23), and COPI at various times after release of the exit block. The quantification is from confocal sections, according to Mironov et al. (2001). Bars are standard errors from the quantification of 20 cells in each case.

(M) VSVG concentration (linear density) at ER exit domains at various times after release of the exit block. Exit domains include both the ERES and the forming saccular carrier and are defined as described by Klumperman et al. (1998). The quantification is from cryosections labeled with immunogold and from epon sections labeled by nanogold (then gold enhanced) at the preembedding step. The linear density of gold particles at exit domains was normalized to the linear density of gold particles on ER membranes. Bars are standard errors from the quantification of 20 cells in each case. At times 0 and 20 min, the quantification was performed only on cryosections.

The scale bars represent 7.5 μm (A–C), 240 nm (D), 300 nm (E and F), and 2.5 μm (G–J).

Correlative Video/Light Electron Microscopy Shows that the Four Carrier Types Correspond to Successive Maturation Stages

Carriers were next examined by both correlative video/light and correlative light electron microscopy (CVEM and CLEM, respectively) to associate the dynamics of each carrier directly with its ultrastructure. HFs and COS7 cells were transfected with VSVG-FP, incubated at 40°C for 12 hr (to accumulate VSVG in the ER), and then shifted to 32°C. At 40°C, VSVG-FP fluorescence showed an ER-like distribution, as expected (not shown). Several seconds after the release of the 40°C temperature block, the motility of the ER mesh increased, and the fluorescence gradually concentrated (2- to 3-fold) into individual spots of less than 1 μm in size. Later, these spots became brighter (5- to 8-fold

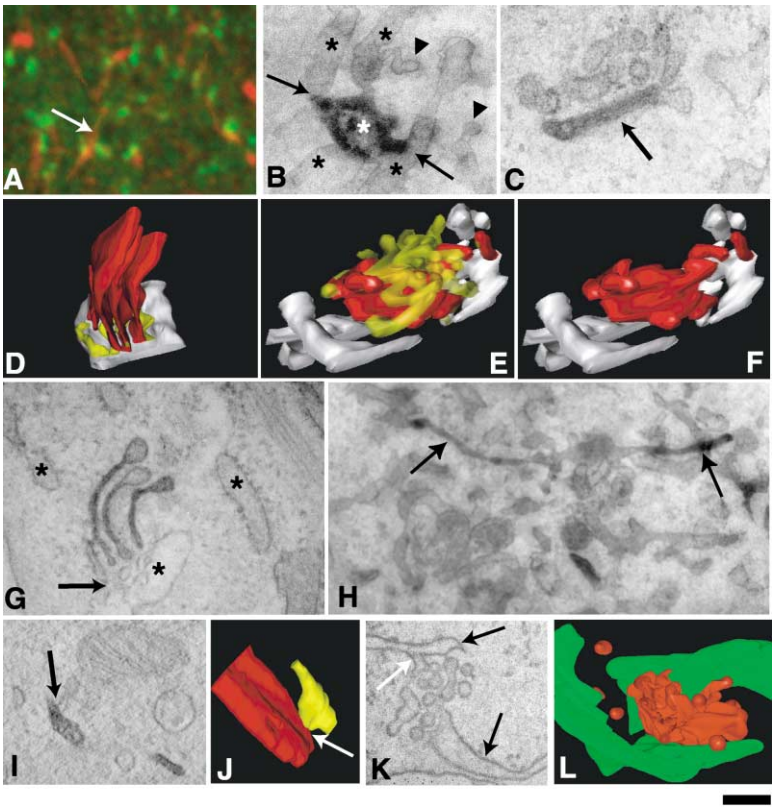

Figure 3. Structure of VSVG-Containing Carriers

COS7 (A, B, and I–L) and RBL (C–H) cells were treated as described in the legend to Figure 2, fixed 10 min after the release of the ER exit block, and prepared for IF or for peroxidase IEM. After IEM labeling, serial sections were prepared and 3D reconstruction and surface rendering were performed.

(A) Concentration of folded VSVG in the peripheral spots (red) is offset from Sec31-positive spots (green). The arrow shows the VSVG-positive tubule.

(B) A type I carrier (white asterisk) widely connected (arrows) to the ER (black asterisks) in the vicinity of an ERES (arrowheads).

(C) Representative serial section of a type II carrier. The arrow shows the EGC positive for VSVG.

(D) Surface rendering (derived from [G]) of a type IV carrier (red) in close vicinity to an ERES (yellow) and the ER (white).

(E and F) Surface rendering (derived from [C]) of a type II carrier (red) in close vicinity to an ERES (yellow in [E], omitted in [F]) and the ER (white).

(G) Type IV carrier with three saccular domains filled with VSVG (DAB precipitate) in close vicinity to an ERES (arrow) and the ER (asterisks).

(H) Type III carriers appearing on a 200 nm tangential section as varicosities (arrows) along a thin radial tubule.

(I and J) Thick (250 nm) sections of carriers labeled for VSVG (DAB precipitate) were cut, prepared for electron tomography, and virtual 2–3 nm slices (e.g., in [I]) were extracted from the tomograms. Three-dimensional reconstruction and surface rendering of the VSVG-containing carrier (red) and the ER (yellow) were performed (see [J]). The arrows in [I] and [J] show the sites of connection between the ER and the VSVG container.

(K) Serial ultrathin (30 nm) sections of a carrier from rapid freezing-cryosubstitution were cut and used to form a 3D reconstruction of the image (see [L]). The black arrows indicate the ER and its connection to the ERES (white arrow).

(L) Saccular container (red) with a blebby surface connected to the ER (green). Six containers were examined by this approach, and they were all connected to the ER.

The scale bars represent 1.5 μm (A), 150 nm (B, C, I, and K), 200 nm (G), and 150 nm (H).

brighter than ER loops), and began to move centripetally along ER loops in an apparently microtubule-dependent manner (see Supplemental Movie 1 at http://www.developmentalcell.com/cgi/content/full/5/4/583/DC1). Interestingly, just before moving, most (~95%) of these large, bright objects emanated a thin and less intensely labeled tubule toward the cell center (Figure 4A). During their centripetal movement they differentiated in either of two types of carriers. One was found more often near the Golgi and was larger and moved slowly, in a stop-and-go (presumably microtubule-mediated) fashion (slow translocating carrier). The other type (mostly peripheral) was smaller, less luminous, and moved more swiftly and directly toward the Golgi (fast translocating carrier).

The cells were then fixed and individual carriers were subjected to 3D reconstruction by correlative microscopy (21 carriers). This showed that carriers just after formation (Figures 4B, 4C, 4H, and 4I) belong to the type I class. Carriers that had already produced a centripetal tubule, which appears to be associated with the beginning of movement (Figure 4E), exhibited a type II structure (a 3D reconstruction is shown in Figure 4J). Fast translocating carriers appeared as varicosities embedded in straight, radially oriented tubules (Figures 4F and 4G), structures which were very similar to type III carriers. Finally, slow translocating carriers exhibited the complex structure classified as type IV: an aggregate of flattened tubular networks and saccules (seemingly stacked, albeit in an irregular fashion), surrounded by round profiles (Figure 4D).

CLEM was also used for the ultrastructural characterization of the carriers as a function of their COPII/COPI labeling. It is known that early forming carriers contain COPII; later, carriers acquire COPI (i.e., label for both COPII and COPI), and, finally, they lose COPII (Scales et al., 1997). Cells were fixed 10 min after release of the temperature block, and therefore, as described above, contained a mixture of carriers of all "ages." The morphology of COPII-labeled (thus, presumably recently formed) carriers is exemplified in Figure 4K. Their ultrastructure appeared to fall into the type I grouping. Carriers containing both COPII and COPI (Figure 4L) were of the structural type II, whereas containers labeling only for COPI exhibited the type IV organization (Figure 4M).

In summary, these results suggest that type I VSVG containers are COPII positive and form through cargo concentration within the lumen of an ER cisterna and the initial protrusion of this domain; type II containers are COPII- and COPI-positive and develop from those

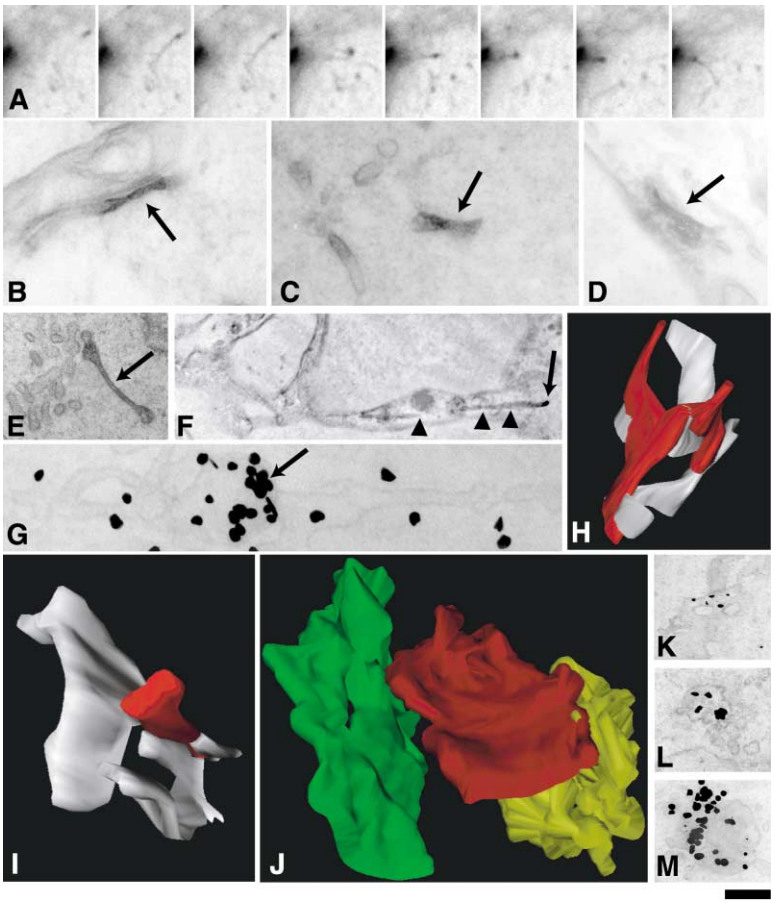

Figure 4. The Carrier Life Cycle by CVEM and CLEM Analyses

COS7 cells were transfected with VSVG-FP, placed in glass-bottomed microwell dishes with coordinated grids, kept for 12 hr at 40°C to accumulate VSVG-FP in the ER, shifted to 32°C to release VSVG from the ER, and then examined by time-lapse analysis under the laser-scanning confocal microscope (A) and prepared for CVEM (B–J). COS7 cells were also grown on dishes with coordinated grids (K–M), treated as described in the legend to Figure 3, fixed, and prepared for CLEM. Next, VSVG, COPII, and COPI were visualized with IF, and COPII-, COPII/COPI-, and COPI-positive carriers were selected after Z stacking under the laser-scanning confocal microscope, and cells were embedded in epon and serially cut, with their subsequent identification at the EM level.

(A) Inverted video frames showing the emanation of thin VSVG-FP-positive tubules from the VSVG-FP-positive spots on their way toward the Golgi.

(B and C) Representative serial sections of type I carriers, which were subjected to 3D reconstruction ([I] and [H], respectively) after their analysis by videomicroscopy. Six other carriers examined at a similar stage in their life cycle all showed a similar ultrastructure.

(D–G) Representative serial sections of a slowly moving, type IV carrier (D); a type II carrier just before its centripetal movement ([E]; three such carriers were examined); and two quickly moving, type III carriers detected under the nucleus (F and G). At the IF level, the last of these (type III) appear as bright varicosities along the less bright fluorescent tubule. Two other carriers of type III exhibiting the same type of mobility were examined.

(H–J) Three-dimensional reconstruction and surface rendering of ER-to-Golgi containers ([H], from [C]; [I], from [B]; [J], from [E]) (red) and ER in white (H and I) or green (J). An ERES is in yellow (J).

(K–M) Examples of COPII-positive ([K], type I), COPII/COPI-positive ([L], type II), and COPI-positive ([M], type IV) carriers identified by CLEM. The scale bars represent 4 μm (A), 140 nm (B, D–F, and K–M), and 100 nm (C and G).

of type I through further protrusion and segregation of the cargo domain from the parent ER cisterna. Both type III (COPI- and COPII-negative) and type IV (COPI-positive) carriers appear to develop from those of type II, concomitant with the beginning of centripetal movement.

PC and VSVG Exit from Different Domains of the Same ERESs

It has been reported recently that transfected PC and VSVG exit the ER at separate ERESs in Vero and HeLa cells (Stephens and Pepperkok, 2002). To examine the relationship between PC and VSVG ERESs, HFs were infected with 045VSV and then both PC and VSVG were blocked and accumulated in the ER. Four and 10 min after release of the block, cells were fixed (see Mironov et al., 2001) and carriers containing PC and VSVG were analyzed by both IF and immuno-EM (IEM; Figure 5). The initial concentration step of PC and VSVG (at 4 min after release) appeared to take place either at distinct ERESs or, more often, in adjoining but nonoverlapping regions of the same ERES (by IF, PC and VSVG spots were very close but nearly completely separated; see Figures 5A–5D). As expected from the observations in Figures 1 and 2, VSVG partially colocalized with COPII (Figure 5I), whereas PC did not (Figure 5J). PC and VSVG were in the same container, but within different domains of this structure (Figure 5K). Later, in the brighter carriers seen 10 min after release, the degree of overlap between PC and VSVG was higher by IF (Figures 5E–5H). Correspondingly, by immuno-EM, VSVG and PC exhibited a higher degree of colocalization at later times after release of the block (Figure 5L). Thus, PC and VSVG concentrate in different domains of the same ERESs, but later converge into the same carrier domain positive for COPI (Figure 5M).

The Formation of ER-to-Golgi Carriers Does Not Involve Vesicle Budding/Fusion but Depends on the Function of COPII

Our above observations are difficult to reconcile with the current idea that carriers form by budding, followed by homotypic fusion of vesicles. We thus examined whether our finding that vesicles near ERESs are few and devoid of cargo might be due to technical limitations. First, additional immunolabeling techniques were used to verify whether limited access of the antibodies

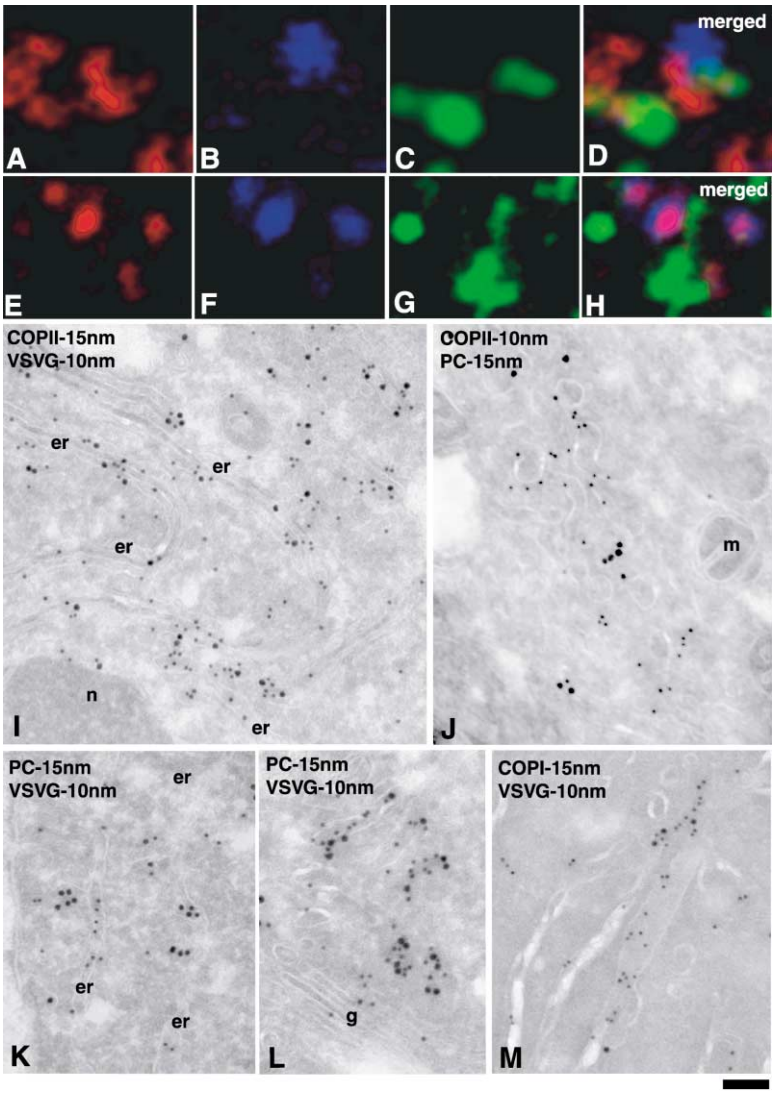

Figure 5. PC and VSVG Are Concentrated in Different Domains of the ER but Move to the Golgi by the Same Transport System

HFs were stimulated to synthesize PC by adding 1% calf serum, then infected with 045VSV and incubated at 40°C for 3 hr in the absence of ascorbic acid to accumulate both PC and VSVG in the ER. Next, cells were shifted to 32°C and 50 μg/ml of ascorbic acid was added back to the medium to release both the temperature and hydroxylation blocks. The HFs were fixed at 0 (not shown), 4 (A–D and I–K), or 10 (E–H, L, and M) min after the temperature shift. Cells were prepared for IF or IEM.

(A–D) Initial concentration (4 min) of folded VSVG (red) and folded PC (blue) in different ER domains adjacent to an ERES (Sec23, green).

(E–H) Coalescence (10 min) of folded VSVG (red) and folded PC (blue) in the carriers in the vicinity of an ERES (Sec23, green).

(I) Colocalization of VSVG (10 nm particles) and COPII (15 nm particles) in the same domains of the ER (presumably exit domains) 4 min after release of the block.

(J) Lack of precise colocalization between PC (15 nm particles) and COPII (10 nm particles) 4 min after the release of the block.

(K) Concentration of VSVG (10 nm particles) and PC (15 nm particles) in different domains of the ERES 4 min after the release of the block.

(L) Colocalization of VSVG (10 nm particles) and PC (15 nm particles) in the same carriers in the vicinity of the Golgi 10 min after release of the block.

(M) Colocalization of VSVG (10 nm particles) and COPI (15 nm particles) in the same carriers 10 min after the release of the block.

er, endoplasmic reticulum; g, Golgi complex; m, mitochondria; n, nucleus.

The scale bars represent 0.3 μm (A–D and E–H), 150 nm (I, K, and M), and 100 nm (J and L).

could be a crucial barrier for detection of a luminal antigen in vesicles. In addition to saponin, different detergents (0.1% Triton X-100, Figure 6A; 0.2% Nonidet P-40, not shown) were used for membrane permeabilization in preembedding experiments. Second, vesicles were examined using an antibody against the cytosolic tail of VSVG, and vesicles were discriminated from cross-sections of tubules by tilting analysis. In all cases, gold particles were associated with saccules and tubules, but not with vesicles and buds (Figures 6B and 6C). Third, a radically different approach was used. Cells were transfected with secretory soluble horseradish peroxidase (ssHRP), the detection of which is free from all of the problems related to antibody access to epitope (Connolly et al., 1994), fixed at steady state (ssHRP cannot be synchronized) 24 hr after transfection, and subjected to the HRP reaction procedure (Connolly et al., 1994). In some cells, DAB precipitate formed a diffuse staining within the ER, so only cells with low levels of ssHRP expression were chosen for observation (Figure 6D). ssHRP was localized in saccules (250–400 nm in diameter) that were connected to the ER and located in the vicinity of ERESs, which were instead mostly devoid of ssHRP (Figures 6E and 6F). The ssHRP saccules strongly resembled the PC and VSVG type I and type II carriers described above, and most likely represent ssHRP containers exiting the ER. In contrast, again, no ssHRP was observed in vesicles. These data confirm that the small diffusible secretory proteins VSVG and ssHRP are depleted in 60 nm vesicles and buds located near the ERESs.

Second, we sought to test whether our failure to observe cargo-laden vesicles might be because such vesicles are too transient to be detected by our experimental design. If this were the case, that is, if COPII-dependent vesicles fuse immediately after formation to generate a saccular container, they should accumulate (and hence should become detectable) when fusion is inhibited; therefore, clusters of vesicles, rather than saccular carriers, should be observed. To test this possibility, membrane fusion was blocked by inhibiting NSF or p97, two proteins controlling cellular fusion events. Anti-NSF antibodies were used first, under conditions shown to be effective in inhibiting membrane fusion (Fukunaga et al.,

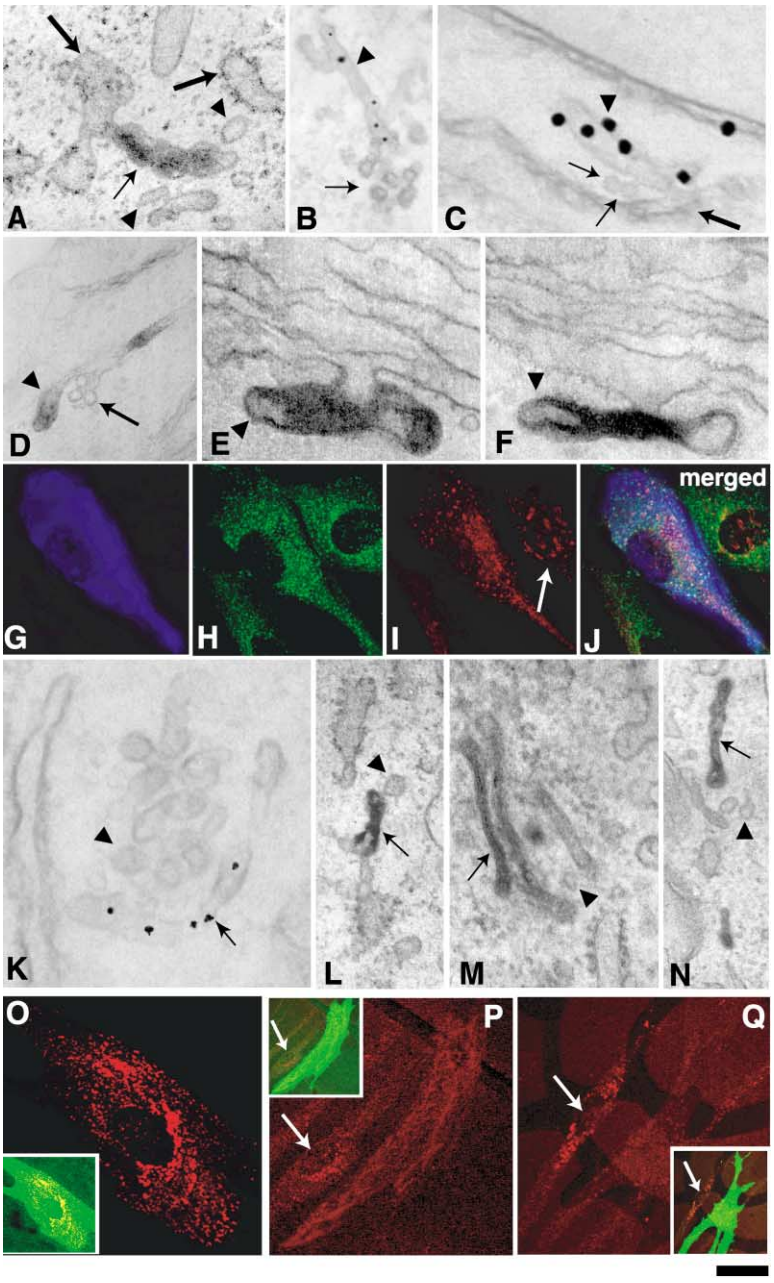

Figure 6. VSVG Exit Does Not Involve 60 nm Vesicles In Vivo but Depends on the COPII Machinery

RBL (A) and COS7 (C–F) cells were treated as described in the legend to Figure 3, or COS7 cells (B) were infected and kept at 32°C for 2 hr. The cells were chemically fixed and prepared for IEM (A–C), or transfected with ssHRP, fixed 24 hr after transfection (at steady state), and then processed for detection of ssHRP (Connolly et al., 1994; D–F).

(A) Permeabilization of cells with 0.1% Triton X-100 neither changes the structure of the VSVG containers (thin arrow) or the ER (thick arrows), nor induces the appearance of labeling in round profiles (arrowheads).

(B and C) VSVG (visualized with the P5D4 monoclonal antibodies against the VSVG cytosolic domain) is concentrated in a saccular domain (arrowhead), which is connected to the ER (thick arrow in [C]), but is not present in round profiles of ERESs (thin arrows). The structure of the VSVG containers (in [B]) at steady state is similar to that after cargo synchronization.

(D–F) ssHRP is present in saccular carriers (arrowheads) but not in profiles of ERESs (arrow in [D]).

(G–J) VSVG (red) is concentrated in the peripheral Sec31-positive (green) spots in NSF antibody-microinjected cells (detected by Cy5; blue in [G]).

Microinjection with anti-NSF and anti-p97 antibodies. BHK cells (G–N) were infected with 045VSV, and after accumulation of VSVG in the ER (see legend to Figure 2) at 40°C, they were microinjected (at 40°C) with the inhibitory anti-NSF (G–J and K–M) or anti-p97 (N) antibodies mixed with anti-mouse Fab fragments conjugated with Cy5 (see Experimental Procedures). After an additional 30 min incubation at 40°C, the cells were shifted to 32°C and fixed after 10 min. Injected cells were found using CLEM (not shown). In mock-injected cells (arrow in [I]), VSVG was also found in the Golgi area. Cells were prepared for IF or IEM (nanogold-enhanced, [K]; immunoperoxidase, [L–N]).

(K–N) Generation of type II (K, L, and N) and type IV (M) carriers. VSVG exiting from the ER concentrates in saccular domains (arrows) of the ERESs. No accumulation of VSVG-containing round profiles (arrowheads) was seen.

(O) Microinjection of wild-type Sar1p does not interfere with the exit of PC (red) from the ER. The inset shows the FITC-dextran that was injected together with Sar1p.

(P and Q) Microinjection of Sar1p-GDP inhibits the exit of PC (red) from the ER. The inset shows the FITC-dextran that was injected together with Sar1p-GDP. The arrow shows a noninjected cell.

Microinjections with GDP-restricted Sar1p. HFs cells were microinjected with tagged versions (see Experimental Procedures) of either wild-type Sar1p or GDP-restricted Sar1p at 40°C. Thirty minutes after microinjection, the exit block was removed and the cells were examined by immunofluorescence 10 min after the shift. A similar trial was performed on VSVG exit from the ER, with similar results.

The scale bars represent 100 nm (A), 140 nm (B and C), 120 nm (D), 60 nm (E and F), 5 μm (G–J and O), 80 nm (K–N), and 10 μm (P and Q).

1998). Because these antibodies are specific for hamster, BHK cells were infected with 045VSV, incubated at 40°C to accumulate VSVG in the ER, microinjected with the anti-NSF antibody at 40°C, and then (after 10 or 30 min of additional incubation at 40°C) shifted to the permissive temperature of 32°C. Four minutes after the shift, VSVG-positive spots were seen in the cell periphery (not shown), and they grew larger over 10 min (Figures 6G–6J). Crucially, CLEM analysis revealed that these spots were not clusters of vesicles; rather, they were typical VSVG-positive type I, type II (Figures 6K and 6L), and type IV containers (Figure 6M). As a positive control, round profiles with a diameter expected for COPI vesicles increased 3-fold in number in the vicinity of the Golgi complex, confirming that the anti-NSF antibody had inhibited vesicle fusion (not shown; see also Mironov et al., 2001). Instead, vesicles in the vicinity of ERESs remained scarce and did not contain VSVG, as

determined by nanogold labeling with an antibody against the cytosolic domain of VSVG (Figure 6K). Similarly, the microinjection of an α-SNAP dominant-negative mutant, which inhibits NSF-mediated fusion (Band et al., 2001), or of an inhibitory anti-p97 antibody (Rabouille et al., 1995) in COS7 cells, did not affect the exit of VSVG from the ER and did not induce accumulation of VSVG-positive vesicles under similar experimental conditions (Figure 6N). Collectively, these data indicate that the formation of large carriers exiting the ER does not require the budding and fusion of small COPII vesicles.

Nevertheless, COPII is essential for export from the ER of all the cargo molecules so far examined (Antonny and Schekman, 2001). To test the role of COPII in the formation of the large PC- and VSVG-containing carriers from the ER, we microinjected Sar1p wild-type (Figure 6O) or a GDP-restricted form of Sar1p (Figures 6P and 6Q) that has previously been shown to inactivate the COPII machinery (see Aridor et al., 2001). Because of the low solubility of these proteins and the need to inject them at high concentrations, we added a short hydrophilic peptide to their N terminus (see Experimental Procedures). Cells were injected 30 min before releasing the exit block, and examined 10 min after the release of the block. The injected Sar1p-GDP mutant markedly inhibited the exit of both PC- and VSVG-containing carriers from the ER, whereas Sar1p wild-type was without effect.

Discussion

This study describes the dynamics and structure of forming and translocating ER-to-Golgi carriers based on the use of CVEM and tomography. The formation of carriers can be summarized as follows (see Figure 7): their appearance begins with the concentration of cargo within domains of the ER adjacent to ERESs (type I in Figures 7A and 7B). Both the ERES and the VSVG (but not the PC) cargo domains are coated with COPII. After (or during) this initial concentration, the cargo-containing domain protrudes from the ER as a large and relatively irregular saccule that remains continuous with the ER (type II in Figures 7C and 7D). Next, the saccular cargo domain is further segregated from the ER, but remains connected to it by short tubules. The cargo-containing sacculus then starts moving toward the center of the cell, and develops into a translocating carrier of either type III (Figures 7E and 7F) or type IV (Figures 7G and 7H). For VSVG carriers, this transition is marked by the complete replacement of COPII with COPI (type IV) or by the loss of coat (type III). The type III and type IV translocating carriers are quite different in terms of dynamics, morphology, and composition. Type IV carriers "wander" relatively slowly through the cytosol in a stop-and-go fashion, comprise two or more saccules (usually loosely stacked) and variable tubular components, and label for COPI. Because they are larger than the static type II containers, they may result from the growth of type II saccules, or from the coalescence of two or more of these. Instead, type III carriers are elongated distensions (about 400 nm long) that are not coated with any COP and move quickly within radial membranous tubules. To our knowledge, this kind of

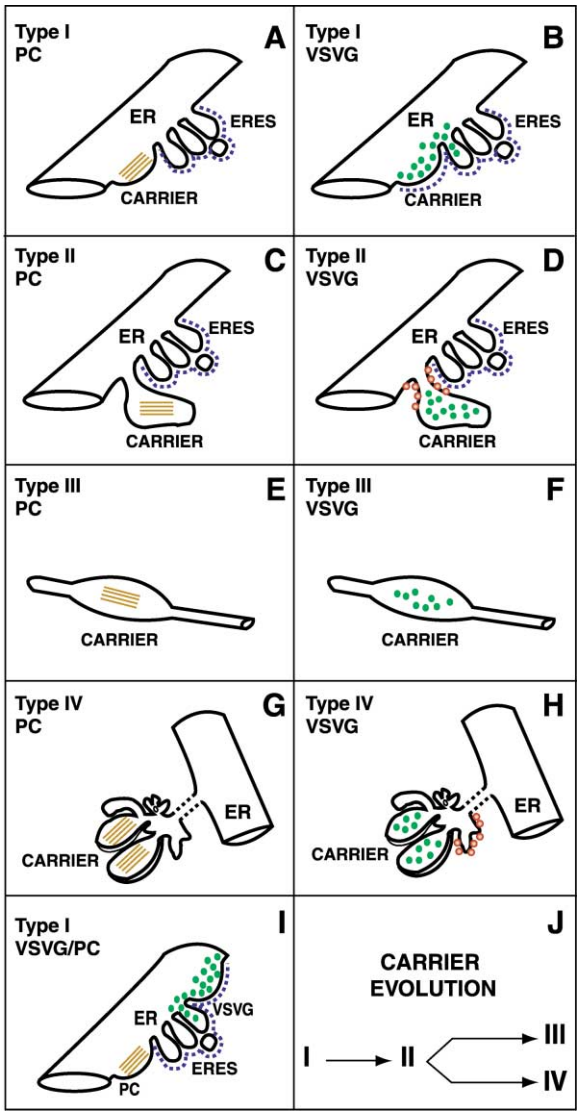

Figure 7. Schematic Representation of ER-to-Golgi Carrier Types

Procollagen is drawn in brown thin lines; VSVG, in green dots; COPII, in blue dashed line; and COPI, in red spheres.

(A and B) Type I. Distended domains of the ER with concentrated cargo are located close (from a few nm to 0.5 μm) to an ERES and are likely to be containers fixed just in the process of appearing from the ER. ERESs (A and B) and VSVG carriers (B) are coated with COPII, while PC carriers (A) are not. PC is excluded from ERESs, whereas VSVG often partially penetrates them.

(C and D) Type II. Flattened and elongated (>300 nm) saccules protruding from, but still in continuity through tubules with, the ER. These develop from type I carriers after protrusion from the ER. COPI is localized at the isthmus of the protruded carrier (D).

(E and F) Type III. Distensions (>300 nm in length) embedded in thin (50–70 nm) tubules devoid of ribosomes, which are usually radially oriented. They appear to be carriers caught during translocation toward the Golgi.

(G and H) Type IV. Larger and more complicated membranes comprising several (two to four) saccules partially stacked and associated with the ER. The association with the ER is represented with a dashed line.

(I) Type I carriers containing both VSVG and PC in the same cell (HF). PC and VSVG do not share the same zone of the ER before exit.

(J) Development of the carriers as inferred from CVEM experiments.

carrier has not been reported previously, possibly because of its small size, low frequency, and rapid movement. The mechanisms by which type II containers develop into type III or type IV translocating carriers are unclear at this time, as is the difference in function, if any, between type III and type IV carriers. A scheme of the evolution of ER-to-Golgi carriers is shown in Figure 7J.

PC- and VSVG-containing carriers are altogether similar, but not identical, at all stages. One difference is that during formation the saccules containing VSVG are covered with COPII, whereas those containing PC are not. Second, PC and VSVG do not appear to concentrate within the same regions of the forming containers at the ERESs. Rather, they localize into separate but adjacent domains of their container (Figure 7I). We hypothesize that the reason for these divergences is that the mechanisms for VSVG and PC recruitment and concentration at ERESs are different. VSVG binds the COPII subunit Sec23/24 (Aridor et al., 2001) through its cytosolic tail. It is therefore logical to presume that it is recruited to the ERESs through such binding (see Aridor et al., 1998). In contrast, as a soluble protein, PC does not bind directly to COPII. In principle it is possible that PC binds to a cargo receptor, for instance one of the p24 proteins, which in turn binds to COPII through its cytosolic tail (Antonny and Schekman, 2001). However, the absence of COPII labeling on PC saccules at all times suggests that this model is unlikely. How then can PC concentrate at exit domains? A scheme could be envisaged that is based on the ER exit mechanism determined for amylase and chymotrypsinogen. These proteins have been proposed to exit the ER by bulk flow (Martinez-Menarguez et al., 1999), and to undergo condensation soon after exit (Warren and Mellman, 1999). It has also been shown that under specific conditions the aggregation of these enzymes can begin in the ER itself (Tooze et al., 2001). We hypothesize that a similar mechanism could apply to the formation of PC carriers; namely, that a first level of PC aggregation might begin in the ER, and that the aggregates themselves might provide a mechanism for protrusion, analogous to the case of secretory granules (Arvan and Castle, 1998). This condensation of PC in the ER may be favored by the creation of a suitable local physical environment, such as low pH, at ERESs (see Warren and Mellman, 1999). Some experimental evidence in support of this possibility exists, as a vacuolar ATPase proton pump has been shown to be present in pre-Golgi carriers, where it is probably recruited to by COPII. Thus, in the case of PC export from the ER, one role of COPII would be to recruit ion or proton pumps (as suggested by Ying et al., 2000) to ERESs, in addition to the SNAREs and other protein machineries needed for later trafficking events (see below).

What is the precise nature and function(s) of the ERESs? There are several lines of evidence indicating that ERESs participate in the formation of the cargo containers, but are not themselves containers that undergo centralization and deliver cargo to the Golgi. One is that they obviously do not contain significant amounts of cargo (PC is completely and VSVG partially excluded; see Figures 1 and 2). Second, as reported by others, ERESs contain both COPII and IC SNAREs such as Sec22 and Bet1 (Klumperman et al., 1998; Chao et al., 1999), but all of these proteins (COPII, Sec22, and Bet1) exhibit a rather stable location and do not exhibit significant centripetal movement (Chao et al., 1999; Hammond and Glick, 2000). Instead, these permanently COPII-positive sites can become associated with cargo protein (VSVG; Stephens et al., 2000) during a cargo concentration step, but they remain peripheral as cargo dissociates from them and moves toward the Golgi. We envision that a key role of the ERESs is to concentrate and store proteins of the fusion machinery (e.g., SNAREs) through binding to COPII. In addition, the ERESs might include microtubule-docking and membrane-bending devices, as well as ion pumps controlling the immediately adjacent luminal environment. At each carrier departure, a suitable complement of this accumulated machinery might be incorporated into the outgoing carrier. Other important roles of COPII at the exit domains might be, in the case of some (probably many) secretory proteins (such as VSVG), to act directly (or via adaptors; see Antonny and Schekman, 2001) to recruit cargo proteins into carriers, or to help bending the membrane of VSVG carriers into a tubular-saccular shape for protrusion out of the ER.

The observations in this study, which are based on a set of high-resolution morphological techniques, speak strongly against the view that in vivo ER-to-Golgi carriers form by budding and fusion of COPII vesicles. Instead, they indicate that these carriers form by progressive extrusion of large ER domains specialized for export. They confirm, however, that the ER exit process absolutely requires COPII for both PC and VSVG export. How can these findings be reconciled with the in vitro evidence that COPII forms 60 nm vesicles (reviewed in Antonny and Schekman, 2001)? Simply put, our hypothesis is that in mammalian cells, the COPII machinery uses its fundamental properties of bending membranes (Aridor et al., 2001) and sorting proteins (Aridor et al., 1998) to recruit cargo and machinery proteins into highly curved membrane regions (the ERES tubules and the tubular-saccular carriers), rather than to form vesicles. However, the situation might be different in yeast, where the smaller size and different environmental conditions might favor a different organization.

An in vivo analysis of the formation of ER-to-Golgi carriers performed by Bannykh et al. (1996) provides a different interpretation of the structure of these carriers, and a more recent study (Horstmann et al., 2002) has reported that carriers formed at 15°C appear as clusters of vesicles, rather than saccules. We believe the latter to be an effect of the 15°C block, during which carriers grow enormously and present a very prominent convoluted tubular component (which could appear vesicular in thin sections). No such structures are seen when carriers form at the physiological temperatures used in our study. Further, Horstmann et al. (2002) have reported that carriers at 15°C are not in continuity with the ER. In our view, the discrepancies between these and our observations can be explained by the fact that these authors did not use tomography techniques, without which it is very difficult to detect continuities or to distinguish buds and vesicles from tubules.

In summary, we find that in living mammalian cells, both PC- and VSVG-containing carriers arise from the

ER by direct and/or indirect COPII-dependent cargo concentration in the vicinity of COPII-coated tubular-vesicular clusters, and by protrusion of these specialized cargo domains, in a process that does not involve budding and fusion of small vesicles. Fully formed carriers then move to the Golgi and evolve into either of two types of translocating carriers that have different kinetic and structural features. These results will hopefully help define the physiological role of the molecular machineries underlying the ER-to-Golgi traffic segment. The challenge is now to reconstitute in vitro the en bloc protrusion mechanism and to identify the regulatory elements responsible for the formation of these large carriers in mammalian cells.

Experimental Procedures

Unless otherwise noted, all chemicals and reagents were obtained from previously indicated sources (Mironov et al., 2001) or from Sigma. Fab fragments of the anti-IgG antibodies were from Jackson ImmunoResearch. The anti-Sec23 antibody was from Affinity BioReagents. The I-14 monoclonal antibody against folded VSVG was from D.S. Lyles (Wake Forest University School of Medicine, Winston-Salem, NC). The anti-p97 polyclonal antibody was from G. Warren (Yale University, New Haven, CT). The cDNA of ssHRP was from D. Cutler (University College, London, UK), cDNAs of wild-type Sar1p and Sar1[T39N] mutant protein were from W. Balch (Scripps Research Institute, La Jolla, CA), and the cDNA of Sec31-GST was from W. Hong (Institute of Molecular and Cell Biology, Singapore); the polyclonal antibodies (LF68) against the C-terminal peptide of the α1 chain of PC was from L.W. Fisher (NIH, Bethesda, MD). The growth of HFs and CEFs, COS7, CHO, NRK, and RBL cells, infection of cells with the 045 strain of vesicular stomatitis virus and their transfection, stimulation of PC synthesis in HFs (kindly provided by M. De Luca, Istituto Dermatologico dell' Immacolata, Rome, Italy), synchronization of cargo movement along the secretory pathway (Bonfanti et al., 1998; Mironov et al., 2001), 3D reconstructions of EM serial sections, CLEM and CVEM, ultrathin cryosectioning, rapid freezing-cryosubstitution, analysis of samples by electron tomography (Mironov et al., 2001), and triple labeling (Brouns et al., 2002) were all carried out as previously described. Microinjection of anti-NSF and anti-p97 polyclonal antibodies was performed (procedure and concentrations of antibodies) as has been described previously (Fukunaga et al., 1998 and Rabouille et al., 1995, respectively). GDP-restricted Sar1p (from G. Egea, University of Barcelona, Barcelona, Spain) and Sar1p wild-type were modified by adding three tags and the hydrophilic peptide YGRLLRRQRRR to their N terminus, purified on a His column, and microinjected at 2 mg/ml. Quantification of colocalization on confocal sections was performed according to Mironov et al. (2001). Organelle definitions were according to Mironov et al. (2001). Quantification of the gold particles on ultrathin sections was performed according to Klumperman et al. (1998).

Supplemental Data at http://www.developmentalcell.com/cgi/content/full/5/4/583/DC1 contains one movie of a living cell. Serial sections, consecutive images of CVEM and CLEM, and 3D reconstructions can be found at our website, http://www.negrisud.it/en/Mironov/movies.

Acknowledgments

We thank A. Fusella, O. Martella, V. Edelman, and R. and E. Polishchuk for technical assistance, M. Capestrano for preparation of the Sar1p constructs, E. Fontana for help with figures, C.P. Berrie for critical reading of the manuscript, and all of the people who provided us with cell lines, antibodies, and cDNA constructs. We acknowledge financial support from the Italian Association for Cancer Research (AIRC, Milan, Italy), Telethon Italia (grant nos. E.0982, E.1105, and E.1249), European network (A.L. and K.N.J.B.), and the Italian National Research Council (contract n. 01.00035.PF49). A.J.K. is supported by the Royal Netherlands Academy of Arts and Sciences (KNAW), and W.J.C.G., and K.N.J.B. by FEI.

Received: April 17, 2003
Revised: August 26, 2003
Accepted: August 26, 2003
Published: October 6, 2003

References

Antonny, B., and Schekman, R. (2001). ER export: public transportation by the COPII coach. Curr. Opin. Cell Biol. *13*, 438–443.

Aridor, M., Weissman, J., Bannykh, S.I., Nuoffer, C., and Balch, W.E. (1998). Cargo selection by the COPII budding machinery during export from the ER. J. Cell Biol. *141*, 61–70.

Aridor, M., Fish, K.N., Bannykh, S., Weissman, J., Roberts, T.H., Lippincott-Schwartz, J., and Balch, W.E. (2001). The Sar1 GTPase coordinates biosynthetic cargo selection with endoplasmic reticulum export site assembly. J. Cell Biol. *152*, 213–229.

Arvan, P., and Castle, D. (1998). Sorting and storage during secretory granule biogenesis: looking backward and looking forward. Biochem. J. *332*, 593–610.

Band, A.M., Maatta, J., Kaariainen, L., and Kuismanen, E. (2001). Inhibition of the membrane fusion machinery prevents exit from the TGN and proteolytic processing by furin. FEBS Lett. *505*, 118–124.

Bannykh, S.I., Rowe, T., and Balch, W.E. (1996). The organization of endoplasmic reticulum export complexes. J. Cell Biol. *135*, 19–35.

Bonfanti, L., Mironov, A., Jr., Martinez-Menarguez, J., Martella, O., Fusella, A., Baldassarre, M., Buccione, R., Geuze, H., Mironov, A., and Luini, A. (1998). Procollagen traverses the Golgi stack without leaving the lumen of cisternae: evidence for cisternal maturation. Cell *95*, 993–1003.

Brouns, I., Van Nassauw, L., Van Genechten, J., Majewski, M., Scheuermann, D.W., Timmermans, J.P., and Adriaensen, D. (2002). Triple immunofluorescence staining with antibodies raised in the same species to study the complex innervation pattern of intrapulmonary chemoreceptors. J. Histochem. Cytochem. *50*, 575–582.

Chao, D.S., Hay, J.C., Winnick, S., Prekeris, R., Klumperman, J., and Scheller, R.H. (1999). SNARE membrane trafficking dynamics in vivo. J. Cell Biol. *144*, 869–881.

Claude, A. (1970). Growth and differentiation of cytoplasmic membranes in the course of lipoprotein granule synthesis in the hepatic cell. I. Elaboration of elements of the Golgi complex. J. Cell Biol. *47*, 745–766.

Connolly, C.N., Futter, C.E., Gibson, A., Hopkins, C.R., and Cutler, D.F. (1994). Transport into and out of the Golgi complex studied by transfecting cells with cDNAs encoding horseradish peroxidase. J. Cell Biol. *127*, 641–652.

Fukunaga, T., Furuno, A., Hatsuzawa, K., Tani, K., Yamamoto, A., and Tagaya, M. (1998). NSF is required for the brefeldin A-promoted disassembly of the Golgi apparatus. FEBS Lett. *435*, 237–240.

Hammond, A.T., and Glick, B.S. (2000). Dynamics of transitional endoplasmic reticulum sites in vertebrate cells. Mol. Biol. Cell *11*, 3013–3030.

Horstmann, H., Ng, C.P., Tang, B.L., and Hong, W. (2002). Ultrastructural characterization of endoplasmic reticulum-Golgi transport containers (EGTC). J. Cell Sci. *115*, 4263–4273.

Klumperman, J. (2000). Transport between ER and Golgi. Curr. Opin. Cell Biol. *12*, 445–449.

Klumperman, J., Schweizer, A., Clausen, H., Tang, B.L., Hong, W., Oorschot, V., and Hauri, H.P. (1998). The recycling pathway of protein ERGIC-53 and dynamics of the ER-Golgi intermediate compartment. J. Cell Sci. *111*, 3411–3425.

Krijnse-Locker, J., Parton, R.G., Fuller, S.D., Griffiths, G., and Dotti, C.G. (1995). The organization of the endoplasmic reticulum and the intermediate compartment in cultured rat hippocampal neurons. Mol. Biol. Cell *6*, 1315–1332.

Ladinsky, M.S., Mastronarde, D.N., McIntosh, J.R., Howell, K.E., and Staehelin, L.A. (1999). Golgi structure in three dimensions: functional insights from the normal rat kidney cell. J. Cell Biol. *144*, 1135–1149.

Lefrancois, L., and Lyles, D.S. (1983). Cytotoxic T lymphocytes reactive with vesicular stomatitis virus: analysis of specificity with monoclonal antibodies directed to the viral glycoprotein. J. Immunol. *130*, 1408–1412.

Martinez-Menarguez, J.A., Geuze, H.J., Slot, J.W., and Klumperman, J. (1999). Vesicular tubular clusters between the ER and Golgi mediate concentration of soluble secretory proteins by exclusion from COPI-coated vesicles. Cell *98*, 81–90.

McIntosh, J.R. (2001). Electron microscopy of cells: a new beginning for a new century. J. Cell Biol. *153*, F25–F32.

Mironov, A.A., Beznoussenko, G.V., Nicoziani, P., Martella, O., Trucco, A., Kweon, H.-S., Di Giandomenico, D., Polishchuk, R.S., Fusella, A., Lupetti, P., et al. (2001). Small cargo proteins and large aggregates can traverse the Golgi by a common mechanism without leaving the lumen of cisternae. J. Cell Biol. *155*, 1225–1238.

Nehls, S., Snapp, E.L., Cole, N.B., Zaal, K.J., Kenworthy, A.K., Roberts, T.H., Ellenberg, J., Presley, J.F., Siggia, E., and Lippincott-Schwartz, J. (2000). Dynamics and retention of misfolded proteins in native ER membranes. Nat. Cell Biol. *2*, 288–295.

Presley, J.F., Cole, N.B., Schroer, T.A., Hirschberg, K., Zaal, K.J., and Lippincott-Schwartz, J. (1997). ER-to-Golgi transport visualized in living cells. Nature *389*, 81–85.

Rabouille, C., Levine, T.P., Peters, J.M., and Warren, G. (1995). An NSF-like ATPase, p97, and NSF mediate cisternal regrowth from mitotic Golgi fragments. Cell *82*, 905–914.

Rambourg, A., and Clermont, Y. 1997. Three-dimensional structure of the Golgi apparatus in mammalian cells. In The Golgi Apparatus, E.G. Berger and J. Roth, eds. (Basel: Birkhauser Verlag).

Sabesin, S.M., and Frase, S. (1977). Electron microscopic studies of the assembly, intracellular transport, and secretion of chylomicrons by rat intestine. J. Lipid Res. *18*, 496–511.

Scales, S.J., Pepperkok, R., and Kreis, T.E. (1997). Visualization of ER-to-Golgi transport in living cells reveals a sequential mode of action for COPII and COPI. Cell *90*, 1137–1148.

Stephens, D.J., and Pepperkok, R. (2002). Imaging of procollagen transport reveals COPI-dependent cargo sorting during ER-to-Golgi transport in mammalian cells. J. Cell Sci. *115*, 1149–1160.

Stephens, D.J., Lin-Marq, N., Pagano, A., Pepperkok, R., and Paccaud, J.P. (2000). COPI-coated ER-to-Golgi transport complexes segregate from COPII in close proximity to ER exit sites. J. Cell Sci. *113*, 2177–2185.

Tooze, S.A., Martens, G.J., and Huttner, W.B. (2001). Secretory granule biogenesis: rafting to the SNARE. Trends Cell Biol. *11*, 116–122.

Warren, G., and Mellman, I. (1999). Bulk flow redux? Cell *98*, 125–127.

Ying, M., Flatmark, T., and Saraste, J. (2000). The p58-positive pre-Golgi intermediates consist of distinct subpopulations of particles that show differential binding of COPI and COPII coats and contain vacuolar H(+)-ATPase. J. Cell Sci. *113*, 3623–3638.